

A novel approach to study the isothermal and non-isothermal crystallization kinetics of Poly(Ethylene Terephthalate) by Raman spectroscopy

K. Ben Hafsia¹ · M. Ponçot¹ · D. Chapron² · I. Royaud¹ · A. Dahoun¹ · P. Bourson²

Received: 30 December 2015 / Accepted: 3 April 2016 / Published online: 14 April 2016
© Springer Science+Business Media Dordrecht 2016

Abstract This paper focuses on the study of the crystallization kinetics of an initially quasi-amorphous Poly(Ethylene Terephthalate) (PET) during controlled heating treatments using Raman Spectroscopy. Characteristic vibrational bands of both crystalline and amorphous phases are then investigated in terms of wavenumber values, full widths at half maximum and integrated intensities variations which led to the establishment of a more accurate crystallinity ratio criterion than the one obtained by standard differential scanning calorimetry (DSC) analysis too much dependent on the low polymer thermal conductivity. Applying this last criterion, isothermal and non-isothermal crystallization kinetics were investigated following the Avrami's and Ozawa's theories in order to identify the germination and growth modes of the triclinic crystals of PET as a function of thermal treatment. Moreover, all the specific microstructural transitions such as cold crystallization, crystallization from the melt, melting and glass transition are detected and characterized. Similar thermal behaviors were obtained from Raman results and conventional differential scanning calorimetry measurements.

Keywords Poly(Ethylene Terephthalate) · In situ Raman spectroscopy · Microstructural transitions · Crystallinity ratio · Crystallization kinetic

Introduction

The Poly(Ethylene Terephthalate) presents important microstructural modifications towards temperature of either its conformation process or its life cycle in use. This thermoplastic polymer may show two main types of microstructure: amorphous and semi-crystalline depending on its thermomechanical history. The amorphous morphology is characterized by the glass transition temperature which illustrates the change of the mechanical behavior from a viscoelastic to a glassy state with decreasing temperature. The semi-crystalline morphology shows, in addition to the glass transition temperature, two supplementary microstructural transitions: crystallization and melting phenomena. Several authors have previously studied the microstructure of such kind of organic materials by using different common experimental technics such as Wide Angle X-rays Scattering (WAXS) [1], Differential Scanning Calorimetry (DSC) [2], Nuclear Magnetic Resonance (NMR) [3], Infra-Red spectroscopy (IR) [4] and Raman spectroscopy [5]. This last technique provides vibrational information related to the conformation and architectural regularity of macromolecular chains. This makes Raman spectroscopy a suitable tool for the microstructural analysis of polymers [6–10]. The amorphous and semi-crystalline vibrational bands have already been well identified in the literature [11, 12]. Many authors have characterized molecular properties of PET using Raman spectroscopy. For instance, Jarvis et al. [13] and Yang et al. [14, 15] studied the macromolecular chains orientation using Raman and Infra-Red spectroscopies. Kawakami et al. [16] worked on the strain induced crystallization process by identifying the development of the transient mesophases in PET during stretching at 70 °C using Raman spectroscopy and X-rays scattering [13–18]. Ponçot [19], Martin [20] and Chaudemanche [21] have also studied the microstructure modifications of various

✉ M. Ponçot
marc.poncot@univ-lorraine.fr

K. Ben Hafsia
khaoula.ben-hafsia@univ-lorraine.fr

¹ Département Science et Ingénierie des Matériaux et Métallurgie, Institut Jean Lamour UMR 7198 CNRS-Université de Lorraine, Parc de Saurupt, CS 50840, 54011 Nancy Cedex, France

² LMOPS, Université de Lorraine, Centrale Supélec, EA 4423, 2 Rue E. Belin, F-57070 Metz, France

polymers by coupling Raman spectroscopy with several characterization techniques and mechanical devices.

Specific singularities which could occur in the Raman spectrum of PET due to the effect of temperature have been already studied and reported in the literature. Most of them are related to vibrational band variations in terms of intensity, wavenumber shift and Full Width at Half Maximum (FWHM) [19, 22, 23]. Melveger [5] and McGraw [24, 25] were the first authors working on crystallinity changes in PET using Raman results by correlating the density of the polymer with the evolution of some characteristic vibrational bands. Melveger [5] considered the $1096\text{ cm}^{-1}/632\text{ cm}^{-1}$ intensity ratio to study the crystallization but it must be only for PET samples having no preferential orientation since the 632 cm^{-1} band intensity changes as a function of the macromolecular chains orientation. Nevertheless, to avoid orientation problems, Bulkin et al. [26] have studied the $1092\text{ cm}^{-1}/1117\text{ cm}^{-1}$ ratio. They showed that this Raman ratio correlates well with the FWHM of the carbonyl stretching band (1725 cm^{-1}) which confirms that these two evolutions describe the same phenomenon. McGraw [24] have studied by Raman spectroscopy different semi-crystalline microstructure of PET by annealing at different times and temperatures to obtain the crystallinity ratio by density measurements. He found that the evolution of the intensities of 1096 cm^{-1} , 857 cm^{-1} and 278 cm^{-1} vibrational bands correlate with the material density too. Meanwhile, Wei et al. [27] studied the fast transitional states of PET quenched at different crystallization states using Ultrafast scanning calorimetry with micro-Raman spectroscopy. Their studies reveal that the intensity evolution of the vibrational band characteristic of the stretching of C(O)-O/C-C/C-C(EG) bonds and the melting enthalpies, as a function of annealing time, are in complete agreement. Nevertheless, they did not use vibrational bands intensities to precisely quantify the evolution of crystallinity ratio and the crystallization kinetics during heating and cooling treatments. Some authors studied the crystallization kinetics of PET by isothermal and non-isothermal crystallization techniques [28–31]. Large ranges of Avrami's and Ozawa's exponents have been obtained extending from 1 to 4 depending on the experimental conditions. Keller et al. [32] studied isothermal crystallization of PET bulk samples from the melt and found Avrami's exponent values in the range from 2 to 4, whereas Mayhan et al. [33] who studied PET thin films found Avrami's exponent values in the range from 1.04 to 1.46 which confirms that this exponent depends on the material shape, crystallization temperature and cooling or heating rates [34]. Papageorgiou et al. [28], Ghasemi et al. [35] and Lee et al. [36] who studied the non-isothermal crystallization of PET from the melt, confirm that the Ozawa's plots should lead to a series of straight lines. Ghasemi et al. [35] considered that the Ozawa's theory should be applied with caution because curvatures appear at higher cooling rates and the slope

(Ozawa's exponent) changes with the temperature. Papageorgiou et al. [28] found that the curvature of the straight lines increases with increasing temperature but the Ozawa's exponent keeps always lower than the Avrami's one even if both theories are performed following the same conditions [37–40].

In this paper, DSC-like thermograms are obtained from Raman spectra focusing on the variations occurring in the FWHM of the carbonyls band during heating and cooling treatments. They reveal all the microstructural transitions of PET (crystallization, melting and glass transition phenomena). A rigorous crystallinity ratio is also proposed and used to study the isothermal and non-isothermal crystallization kinetics applying Avrami's and Ozawa's theories. Avrami's and Ozawa's exponents are finally estimated and compared with those obtained by conventional differential scanning calorimetry, in order to compare results with literature and to reveal the right nucleation and crystal growth modes of a 2 mm thick extruded plates of PET.

Material and experimental setups

Material: Poly(Ethylene Terephthalate), PET

The material used in this work is a Poly(Ethylene Terephthalate) produced by BAYER and commercialized by Loraplast under the reference *Axpet® clear 099*. It is provided as 2 mm-thick extruded plates. According to Differential Scanning Calorimetry (DSC) analysis performed at a constant heating rate of 5 °C/min , samples exhibits a glass transition temperature (T_g) at 76 °C , a melting temperature (T_m) at 248 °C and a cold crystallization temperature (T_{cc}) at 125 °C . The initial degree of crystallinity of the extruded plates is about 3 % using the following formulae: $X_c = \frac{\Delta H_m - \Delta H_{cc}}{\Delta H_m^0}$. The theoretical enthalpy of fusion for a perfect crystal of infinite size is taken as $\Delta H_m^0 = 140\text{ J/g}$ [37, 38]. Wide-angle X-ray scattering (WAXS) analysis confirms this small amount of crystals and informs about an isotropic distribution of the macromolecular chains whatever the spatial direction that could be induced by the extrusion process.

Experimental setup

The Raman spectrometer used in this study is a "RXN1" manufactured by Kaiser Optical Systems. This spectrometer is equipped with optical fibers allowing the use of a delocalized probe. The laser diode is used as a light source and produces a monochromatic exciting radiation with a wavelength of $\lambda = 785\text{ nm}$ (Laser power 400 mW). This wavelength is adapted to the study of polymer materials because it eliminates part of the fluorescence emission that could

degrade the Raman signal quality. Its wavenumber range is between 100 cm^{-1} to 3500 cm^{-1} but the studied range of wavenumbers is limited in this study between 500 cm^{-1} to 2000 cm^{-1} . The spectral resolution is 1 cm^{-1} . The Raman acquisitions were performed using the “iC Raman 4.1” software. All spectra were adjusted by spectral deconvolution procedure using Gaussian and Lorentzian functions to fit the vibrational bands of amorphous and semi-crystalline phases, respectively.

The Raman spectrometer is then coupled to a Differential Scanning Calorimetry set up (DSC) in order to acquire in situ the PET vibrational signature at the same time as well-controlled thermal treatment [27, 39, 40]). A specific probe was designed by Kaiser Optical Systems to perfectly accommodate the DSC sample oven.

Calorimetric data were recorded using a Q200 device commercialized by TA-Instruments and analyzed by TA Universal Analysis Software. The experimental errors on the measurements of the enthalpies and temperatures are about $\pm 1\%$ and $\pm 1\text{ }^\circ\text{C}$, respectively. The thermal analysis is recorded under an inert azote atmosphere at a flow rate of 50 ml/min . The DSC device was calibrated by keeping the Raman laser on during the whole scan. This way, the laser power does not influence the measurements of the differential heat flow between the reference and the sample ovens. Samples were shaped to perfectly fit with the geometry of the pans in order to always keep the same analyzed volume fraction of the material even when it melts. The sample weights were close to 20 mg . The standard thermal cycle (heating-cooling-heating) applied to the material was performed at a constant rate of $5\text{ }^\circ\text{C/min}$ in the range from $40\text{ }^\circ\text{C}$ to $300\text{ }^\circ\text{C}$.

Isothermal and non-isothermal crystallization kinetics were studied using the following experimental parameters:

- Isothermal crystallizations were performed on the one hand by heating the sample to $115\text{ }^\circ\text{C}$, $120\text{ }^\circ\text{C}$ and $125\text{ }^\circ\text{C}$ from the glassy state and on the other hand by cooling to $200\text{ }^\circ\text{C}$, $205\text{ }^\circ\text{C}$ and $210\text{ }^\circ\text{C}$ from the melt at a constant rate of $5\text{ }^\circ\text{C/min}$. The material has not been heated to the melt before these thermal treatments in order to enlighten the effect of the initial morphology on the nucleation and growth modes.
- Non-Isothermal crystallizations were performed by cooling the sample from the melt at different cooling rates (2.5 , 5 , 10 , 15 and $20\text{ }^\circ\text{C/min}$) to $40\text{ }^\circ\text{C}$ (the end of the crystallization phenomenon).

To follow the crystallinity ratio and the vibrational signature of the material by Raman spectroscopy, the acquisition parameters of Raman spectra have been determined in order to allow recording one spectrum every Celsius degree during heating or cooling. The acquisition times for each thermal treatment are summarized in Table 1.

Table 1 Spectral acquisition times for each heating and cooling rate

Heating/Cooling rate ($^\circ\text{C/min}$)	Acquisition time (s)	Acquisition interval (s)
2.5	22	24
5	10	12
10	8	10
15	6	8
20	4	6

For isothermal crystallization, the data of polymer crystallinity kinetic are extracted using the most widely used method based on Avrami’s equation (Eq. 1) [41–43].

$$1-X_c(t) = \exp(-K.t^n) \quad (1)$$

where $X_c(t)$ is the crystallinity ratio at a time t , K is the constant crystallization rate and n is the Avrami’s exponent which depends on the nucleation and the geometry of growth of the crystalline form.

In order to describe the evolution of the crystallinity during non-isothermal crystallization, Ozawa’s analyses were performed. According to this theory [28, 44], the non-isothermal crystallization is a result of a large number of small isothermal crystallization stages. Parameters of polymer crystallization kinetic according to Ozawa’s theory were extracted from the following equation (Eq. 2):

$$1-X_c(t) = \exp\left(\frac{-K(T)}{C^m}\right) \quad (2)$$

where $X_c(t)$ is the crystallinity ratio at a time t , $K(T)$ is the cooling function at a temperature T , C is the constant cooling rate and m is the Ozawa’s exponent which depends on the nucleation and the geometry of growth of the crystalline form.

For both isothermal and non-isothermal crystallization, the crystallinity ratio is plotted as a function of the temperature. In order to determine the Avrami’s and Ozawa’s parameters, a linearization of the crystallinity evolutions was done applying a double-logarithmic form to the above described equations.

Experimental results and discussion

Identification of the specific signatures of the amorphous and semi-crystalline microstructure of PET by Raman spectroscopy

Raman spectra of both quasi-amorphous and semi-crystalline PET are presented in Fig. 1. The semi-crystallized material was obtained by annealing of the initial quasi-amorphous material at the cold crystallization temperature of $125\text{ }^\circ\text{C}$ for 24 h to ensure a maximal degree of crystallinity of 29% as revealed

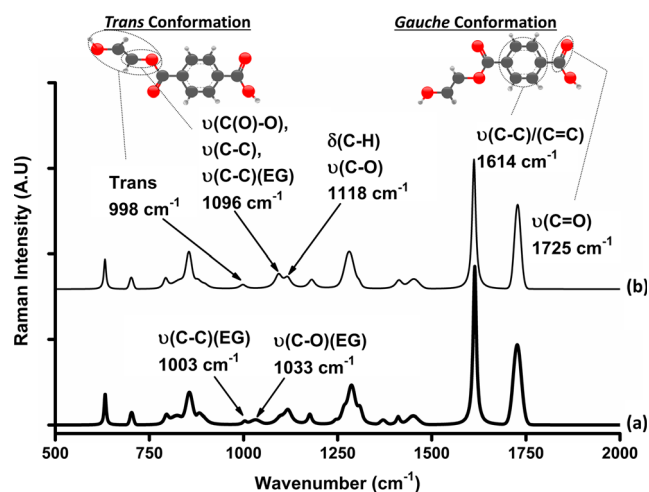


Fig. 1 Identification of the specific vibrational signatures for (a) amorphous and (b) semi-crystalline PET revealed by Raman spectroscopy

by DSC and WAXS post-analysis. The spectra of Fig. 1 enlighten the characteristic vibrational bands peculiar to these two microstructures since Raman spectroscopy is really sensitive to the molecular conformations of PET [5, 11, 16, 26, 45, 46].

Regarding the architecture of PET macromolecules, they can arrange themselves following two different conformational states: “*Trans*” and “*Gauche*” either of the ethylene glycol (EG) segment or of the ester function. It was reported in the literature that PET is able to crystallize only under a global “*Trans*” conformation state of both segments [45, 47]. In the opposite, the amorphous morphology is made of a major fraction of “*Gauche*” conformations but can contain also “*Trans*” one [25, 48, 49].

The vibrational bands assignment can be done easily from the numerous data encountered in the literature [5, 11, 16, 26, 45, 46]. The 1725 cm^{-1} vibrational band is one of the two most intense in the PET spectra and corresponds to the stretching of the C = O bond of the terephthalic acid. This band is narrower in the semi-crystalline material spectrum than in the one of the quasi-amorphous [11]. Its Full Width at Half Maximum (FWHM) can be correlated to the polymer density [5, 50]. The 1614 cm^{-1} vibrational band is assigned to the (C-C/C = C) in plane stretching of the benzene ring [5, 11, 51]. The 1003 cm^{-1} and 1033 cm^{-1} are two characteristic vibrational bands of the “*Gauche*” conformation of the molecular structure (Fig. 1). The bands are then characteristic of the amorphous form and represent respectively the C-C and C-O stretching at the ethylene glycol unit [11]. Once the material is wholly crystallized, the 998 cm^{-1} vibrational band characteristic of the “*Trans*” conformation of the ethylene glycol appears as a substitute of the two previous bands [51]. The most significant change that falls within the context of our study is the vibrational variations of 1096 cm^{-1} and 1118 cm^{-1} vibrational bands from the amorphous to the

semi-crystalline form. The 1118 cm^{-1} band, considered as a reference, characterizes the C-H rocking in the benzene ring and the C-O stretching in the ethylene glycol unit [49, 51, 52]. The 1096 cm^{-1} band characterizes the combination of C(O)-O/C-C/C-C (EG) symmetric stretching bonds and describes the evolution of the conformation from “*Gauche*” to “*Trans*” [45, 53].

Table 2 gathers some characteristic vibrational bands of PET that will be especially focused on for our further studies.

Figure 2 shows the evolution of the 1096 cm^{-1} vibrational band from the glassy amorphous state at 40 °C to the semi-crystalline state at 190 °C just before melting. The 1096 cm^{-1} vibrational band intensity increases with increasing temperature which enlightens the initially quasi-amorphous PET crystallization. From these observations, the estimation of the PET degree of crystallinity is obtained during DSC controlled thermal treatments. The changes that occur in the 1096 cm^{-1} and 1118 cm^{-1} vibrational bands have already been correlated by Everall et al. in 1994 with the evolution of the material density characterized by the FWHM evolution of the 1725 cm^{-1} vibrational band [54]. However, the intensities of the two previous considered vibrational bands were not yet considered to elaborate a ratio able to follow with a good accuracy the real evolution of the PET crystallization.

Equation 3 is considered as the Raman ratio able to describe the evolution of crystallinity:

$$\frac{I_{\bar{\nu}(1096 \text{ cm}^{-1})}}{I_{\bar{\nu}(1118 \text{ cm}^{-1})} + I_{\bar{\nu}(1096 \text{ cm}^{-1})}} \quad (3)$$

where $I_{\bar{\nu}(1096 \text{ cm}^{-1})}$ and $I_{\bar{\nu}(1118 \text{ cm}^{-1})}$ are respectively the intensities of the 1096 cm^{-1} and 1118 cm^{-1} vibrational bands.

Considering this Raman vibrational bands ratio, crystallization evolution shows a similar shape with the one obtained by conventional DSC (crystallization enthalpy evolution). However, an important overestimation appears of about 30 %. It is known that the studied PET presents a small initial fraction of crystalline phase (degree of crystallinity close to 3 %). However, it cannot explain this large difference. So, Fig. 3 compares the Raman spectra of the studied quasi-amorphous PET to the one in case of a 100 % amorphous PET (obtained after fast cooling from the melt).

Table 2 Assignments of characteristic vibrational bands for Poly(ethylene terephthalate)

Raman vibrational bands	Chemical bond	Vibrations
1096 cm^{-1}	C(O)-O/C-C/C-C (EG)	Symmetric stretching
1118 cm^{-1}	C-H/C-O	Rocking/Stretching
1614 cm^{-1}	C-C/C = C	Ring symmetric stretching [5, 11, 51]
1725 cm^{-1}	C = O	Stretching [11, 50]

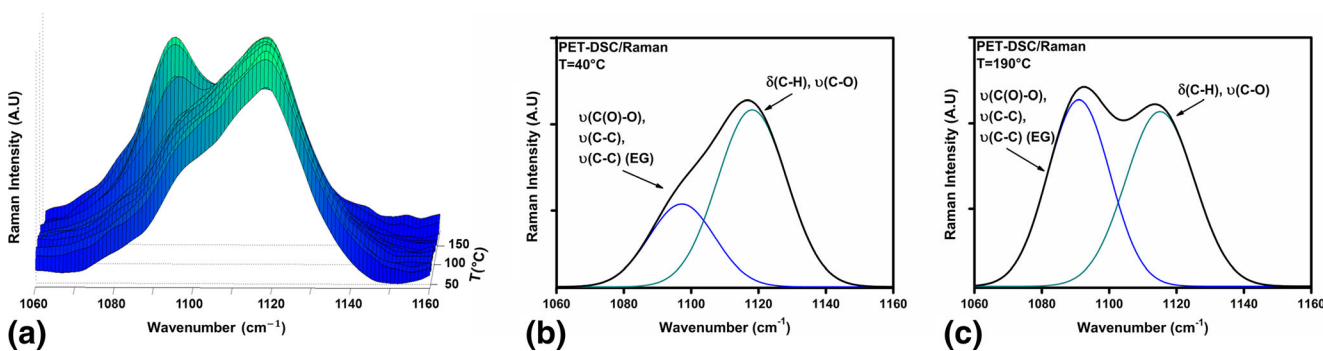


Fig. 2 Focus on the wavenumbers range 1060 cm^{-1} – 1160 cm^{-1} . **a** Evolution as a function of temperature from 40 $^{\circ}\text{C}$ to 190 $^{\circ}\text{C}$ at 5 $^{\circ}\text{C}/\text{min}$ of the Raman spectra of the initially quasi-amorphous PET, **b** quasi-amorphous PET Raman spectra at 40 $^{\circ}\text{C}$, **c** semi-crystalline PET Raman spectra at 190 $^{\circ}\text{C}$

In Fig. 3 (a), at 40 $^{\circ}\text{C}$, the intensity of 1096 cm^{-1} vibrational band is higher than the one observed in Fig. 3 (b) which illustrates the 1096 cm^{-1} and 1118 cm^{-1} bands at 40 $^{\circ}\text{C}$ in case of 100 % amorphous PET. As a conclusion, in case of 100 % amorphous PET, the 1096 cm^{-1} vibrational band still exists and exhibits an initial intensity value ($I_{\bar{\nu}(1096 \text{ cm}^{-1})a}$) which has to be also taken into account in Eq. 3. A Raman criterion taking into account these initial values of the 1096 cm^{-1} vibrational band is presented in Eq. 4 and can be considered as an accurate expression allowing the quantitative determination the degree of crystallinity of PET:

$$r_c^{Raman} = \frac{I_{\bar{\nu}(1096 \text{ cm}^{-1})} - I_{\bar{\nu}(1096 \text{ cm}^{-1})a}}{I_{\bar{\nu}(1118 \text{ cm}^{-1})} + I_{\bar{\nu}(1096 \text{ cm}^{-1})}} \quad (4)$$

where $I_{\bar{\nu}(1096 \text{ cm}^{-1})}$, $I_{\bar{\nu}(1096 \text{ cm}^{-1})a}$ and $I_{\bar{\nu}(1118 \text{ cm}^{-1})}$ are the intensities of the 1096 cm^{-1} , 1096 cm^{-1} in the 100 % amorphous state and 1118 cm^{-1} vibrational bands respectively.

The evolutions of r_c^{Raman} and degree of crystallinity determined simultaneously by DSC as a function of the temperature are plotted in Fig. 4(a). A good correlation is now observed (Fig. 4(b)) in terms of shape and value. Only a slight shift to higher temperatures can be noticed in case of DSC results and can be explained by the fact that Raman

spectroscopy data are acquired in a more reactive way than those obtained by DSC and moreover Raman spectroscopy is sensitive to the change of PET conformations whereas DSC is not. Hence, Raman results seem to be more accurate than those obtained by DSC.

Monitoring of the PET microstructural transitions by Raman spectroscopy in real time during thermal treatments

To monitor the microstructural transitions of the PET during a constant heating scan at 5 $^{\circ}\text{C}/\text{min}$ from 40 $^{\circ}\text{C}$ to 300 $^{\circ}\text{C}$, FWHM and positions of the 1614 cm^{-1} and 1725 cm^{-1} vibrational bands were investigated. Figure 5 illustrates their both evolutions as a function of temperature. The position of the symmetrical stretching vibration of the C-C/C = C bond of the benzene ring shifts linearly to smaller wavenumbers from 1614 cm^{-1} to 1609 cm^{-1} with the increase of temperature (Fig. 5(a)). By contrast, the position of the stretching vibration of the C = O ester bond shifts to higher wavenumbers from 1725 cm^{-1} to 1727 cm^{-1} until the temperature range of 120 $^{\circ}\text{C}$ –125 $^{\circ}\text{C}$ corresponding to the characteristic temperature range of the cold crystallization process (Fig. 5(b)). Then, from 130 $^{\circ}\text{C}$ and 235 $^{\circ}\text{C}$, the position keeps constant at 1727 cm^{-1} until the

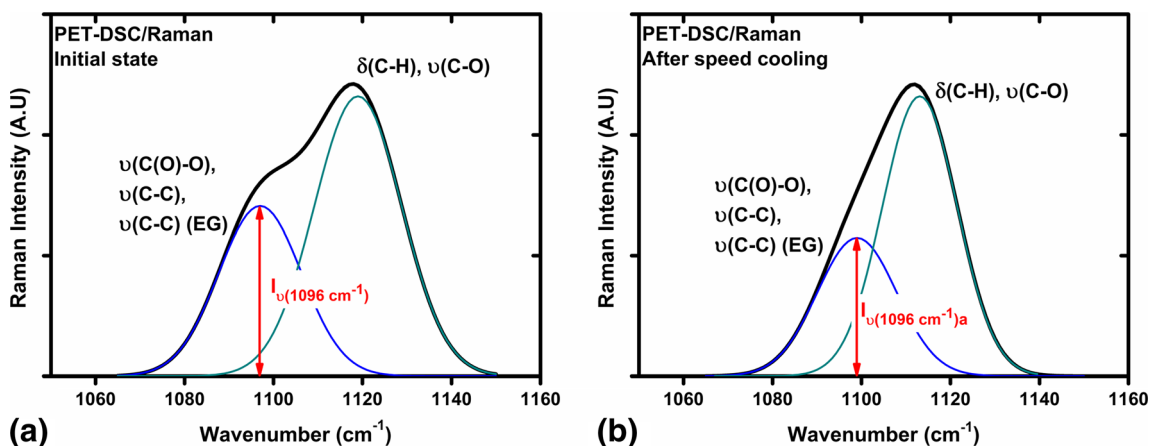


Fig. 3 Illustration of the contribution of the initial crystallinity ratio of the studied PET in the Raman spectrum: **a** 1096 cm^{-1} and 1118 cm^{-1} bands of the quasi-amorphous PET and **b** 1096 cm^{-1} and 1118 cm^{-1} band of 100 % amorphous PET

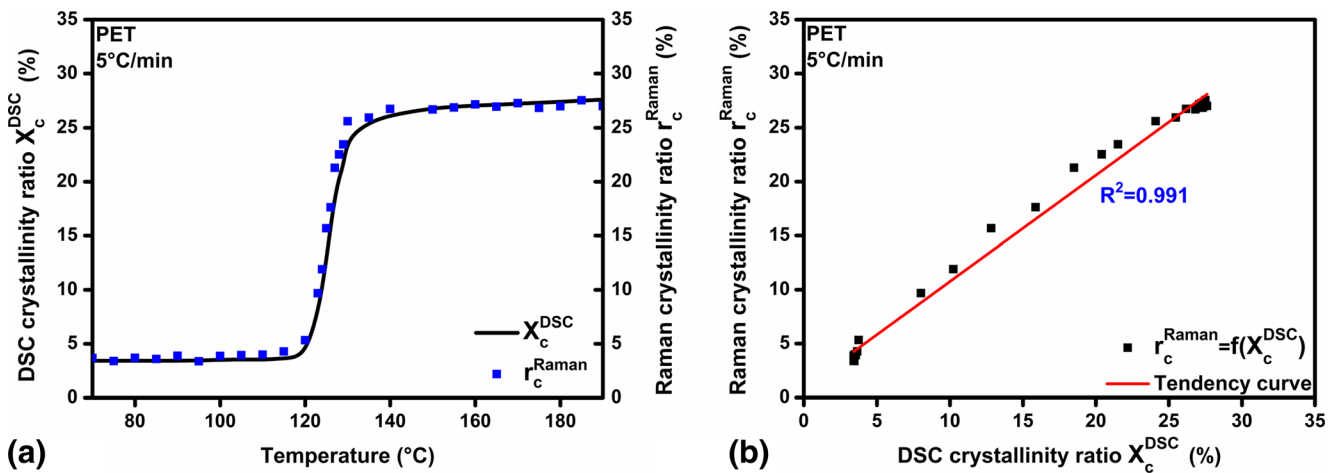


Fig. 4 a Evolutions of the crystallinity ratio by Raman Spectroscopy and DSC, **b** Correlation curve between Raman and DSC results

melting. Once passed through, it reaches the 1731 cm^{-1} final position. Figure 5(c) shows the evolution of the FWHM of the 1614 cm^{-1} vibrational band which increases almost linearly from 11 cm^{-1} to 15 cm^{-1} with increasing temperature from $40\text{ }^\circ\text{C}$ to $300\text{ }^\circ\text{C}$. Figure 5(d) shows the FWHM evolution of the carbonyl vibrational band which keeps constant at 26 cm^{-1} until $120\text{ }^\circ\text{C}$. Then, the FWHM decreases considerably to 21 cm^{-1} in the temperature range of $120\text{ }^\circ\text{C}$ to $125\text{ }^\circ\text{C}$ which

corresponds to the cold crystallization process. This last value is kept constant until $235\text{ }^\circ\text{C}$. In the range of melting temperature ($235\text{ }^\circ\text{C}$ – $250\text{ }^\circ\text{C}$) the FWHM of carbonyl increases and reaches its initial state at 26 cm^{-1} (Fig. 5(d)).

Shifts of bands position to higher or lower values are due to mechanical and/or thermal overloads leading to the compression (higher wavenumbers) or the stretching (lower wavenumbers) of the molecular bonds. This evolution of the

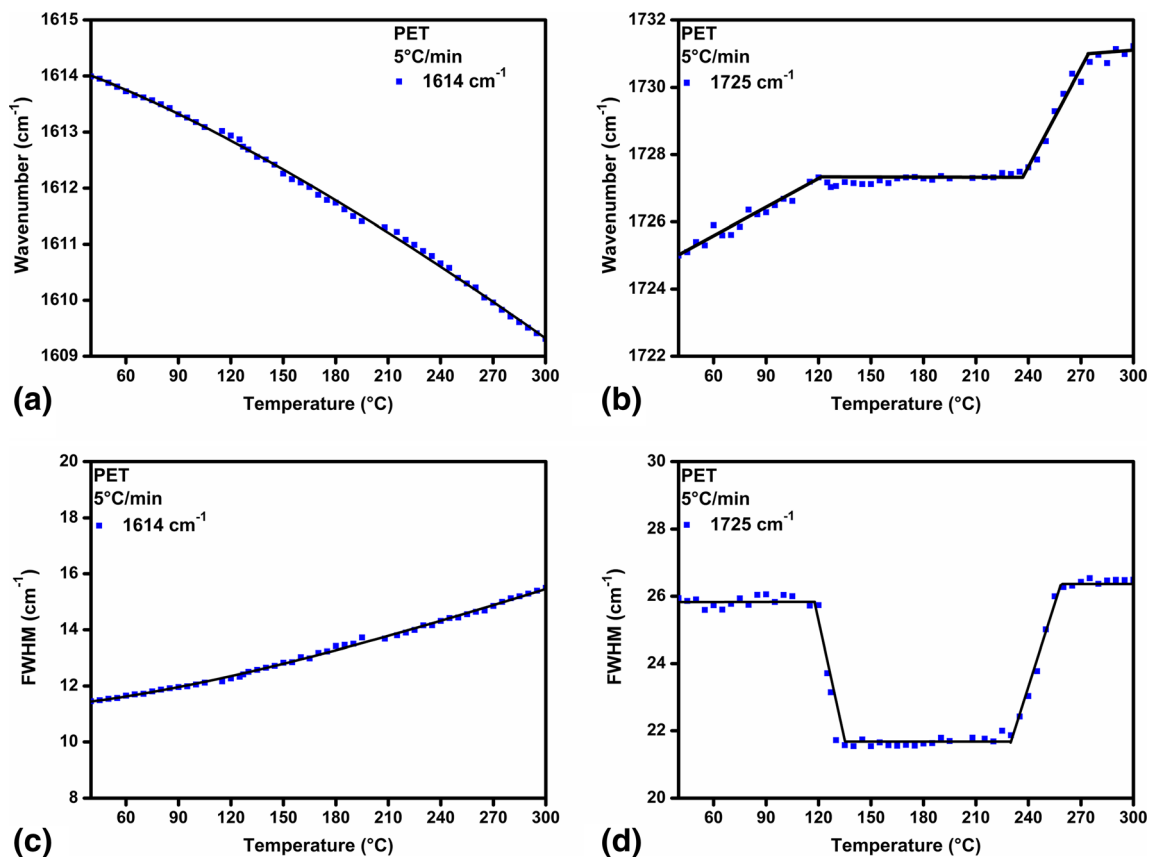


Fig. 5 During a constant heating rate of $5\text{ }^\circ\text{C}/\text{min}$: **a**, **b** Evolutions of the 1614 cm^{-1} and 1725 cm^{-1} vibrational bands position, respectively and **c**, **d** FWHM evolutions of the 1614 cm^{-1} and 1725 cm^{-1} vibrational bands, respectively

C = O vibrational band indicates a two time compressive state due to the temperature increase and the changes in the geometrical structure of the monomeric unit from a disordered amorphous phase to a regular crystalline state (Fig. 5(b)). Due to their location, on both sides of the axis of the PET macromolecule, these carbonyl bonds undergo an internal stress due to the molecular arrangement to “*Trans*” conformation at the cold crystallization temperature. The position then keeps constant because the material reaches its maximum crystallinity ratio. On the other side, the (C-C/C = C) vibrational band shifts to the lower wavenumbers (Fig. 5(a)). This downward trend, characterizes the stretching of the (C-C/C = C) bonds due to the temperature increase to the crystallization zone inducing the arrangement of the PET molecule along the same axis. After the cold crystallization process and approaching the melting temperature, an opposite trend of the two positions is expected. But a second compressive state is observed in the case of the carbonyl groups vibrational band and the (C-C/C = C) vibrational band continues moving towards low wavenumbers. As decoupling mechanical and thermal contributions is difficult, these trends are due to both the thermal effect and to the internal stress occurring in the PET macromolecule [55, 56]. The evolution of these two vibrational bands to high wavenumbers for the carbonyl vibration and to low wavenumbers for (C-C/C = C) vibrational band is due to a possible balance between melting and recrystallization phenomenon occurring simultaneously at the melting process.

FWHM of specific vibrational bands is related to static and dynamic environmental disorder occurring in the material structure. Indeed, a narrow peak corresponds to a regular spatial organization which characterizes a semi-crystalline form of the polymer whereas a broad peak corresponds to a disordered structure corresponding to the amorphous state [53, 57]. So, the FWHM can be correlated with the total density which means that it may describe the evolution of the crystallinity of the material. The changes that occur in the terephthalate segment of the PET molecule are responsible for the amorphous or semi-crystalline phases. Indeed, the carbonyl groups symmetrically placed in the same plane as the benzene ring are in “*Trans*” conformation in the semi-crystalline state. This configuration is characterized by its regularity implying a narrow C = O vibrational band (Fig. 5(d)). By increasing the temperature, the molecular mobility becomes easier which leads to some rotation of the carbonyl groups out of the benzene plane. Each rotational state is represented by a different vibrational stretching frequencies which may be responsible of the broadening of the C = O band in comparison to the crystalline state [48, 58]. Approaching the cold crystallization temperature, the carbonyl groups tend to be in a “*Trans*” conformation in the same plane as the benzene ring and the bandwidth of the C = O stretching vibration becomes narrower. Figure 5(c) shows that the bandwidth of the C-C/C = C stretching vibration (1614 cm^{-1}) is not sensitive to the characteristic temperatures

because of the planarity of the benzene ring which is maintained in both amorphous and crystalline phases.

Regarding the evolution of the 1725 cm^{-1} FWHM of Fig. 5(d), its derivative as a function of temperature is plotted in Fig. 6. The DSC thermogram obtained in situ is also given. Perfectly similar shapes are observed. Thus, it is shown that the $\frac{d(\text{FWHM})}{dT}$ allows the determination of the characteristic temperatures of the material, glass transition, cold crystallization and melting which corresponds exactly to the characteristic temperatures determined by DSC (onset, maximum and endpoint).

$\frac{d(\text{FWHM})}{dT}$ and the heat flow are also plotted as a function of temperature at different heating rates in order to confirm the determination of the characteristic temperature by Raman spectroscopy (Fig. 7). Both by DSC and Raman spectroscopy, the glass transition and the cold crystallization temperatures increase and the melting temperatures decrease with increasing the heating rates. These evolutions confirm that FWHM is sensitive to macromolecular changes occurring during thermal treatments. The characteristic temperatures determined by DSC and Raman spectroscopy are presented in Table 3.

The temperatures determined by both DSC and Raman spectroscopy are the same. In addition the difference between the areas of the melting and the cold crystallization peaks for both heat flow and $\frac{d(\text{FWHM})}{dT}$ curves gives the same value which means that we are able to determine the crystallinity ratio of our material only by realizing Raman scans.

Study of the crystallization kinetics of the PET by Raman spectroscopy

Isothermal and non-Isothermal crystallizations were performed to study the crystallization kinetics of PET applying the previously proposed Raman crystallinity ratio criterion.

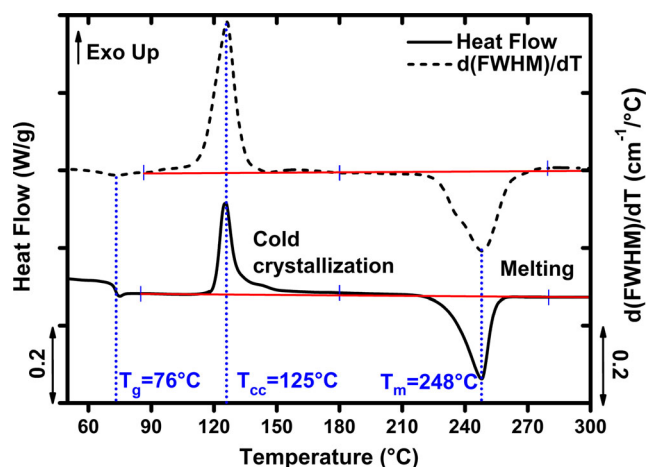


Fig. 6 Comparison between the DSC thermogram and the differential evolution of FWHM of the 1725 cm^{-1} vibrational band $\frac{d(\text{FWHM})}{dT}$ (derivative of Fig. 5 (d) curve) plotted as a function of temperature at a constant heating rate of 5 °C/min

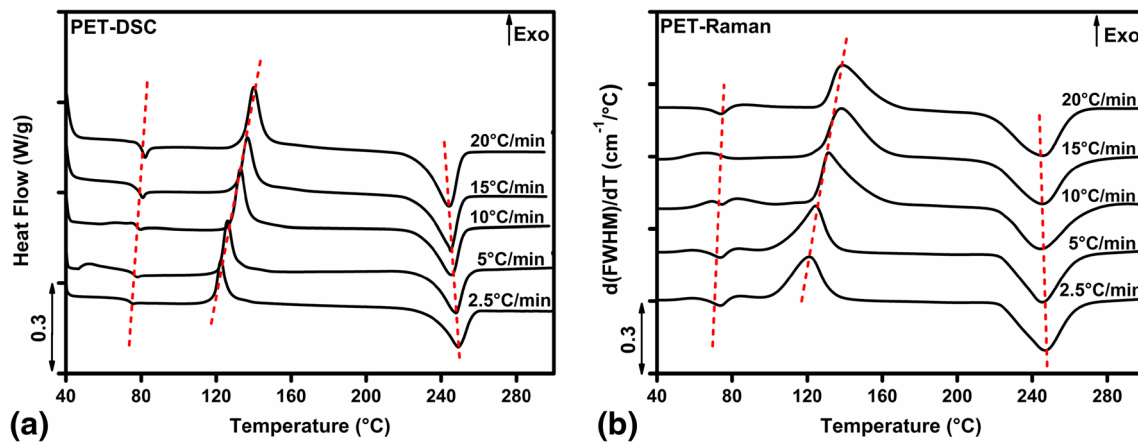


Fig. 7 a Heat flow and b $\frac{d(\text{FWHM})}{dT}$ as a function of temperature at different heating rates

Isothermal crystallization

In order to characterize the crystallization kinetics of PET by Raman spectroscopy, a classical isothermal crystallization using the Avrami theory is used to validate the proposed Raman crystallinity criterion and test if the Raman results are in agreement with those obtained by the DSC method.

These two different methods are used in order to study the thermal response of the material from the glassy state due to the presence of initial crystallites ($X_c = 3\%$) and from the melt after eliminating its thermal history. From the glassy state, the material is annealed at 115 °C, 120 °C and 125 °C just before the cold crystallization temperature (Fig. 8(a)). From the melt, the material is cooled at a constant cooling rate of 5 °C/min and then maintained at 210 °C, 205 °C and 200 °C just above the cold crystallization temperature (Fig. 8(b)).

Both methods show similar evolutions. These observations confirm once again that the considered ratio r_c^{Raman} describes well the real evolution of the crystallinity and that the Raman results are sensitive to the temperature at which the material is annealed or cooled. In order to determine the nucleation/germination modes, the Avrami's equation is then double-linearized by considering a standard method consisting of plotting the data on the logarithmic scale. The results of both methods (from the glassy state and from the melt) determined by Raman spectroscopy and confirmed by DSC are shown in Fig. 9.

Using Eq. 1 for the isothermal crystallization performed from the glassy state (Fig. 9(a) and (b)), the resulting curves show straight lines with a slope n . Unlike those obtained by cooling from the melt (Fig. 9(c) and (d)) which describe a two stage behavior. The first stage corresponds to the primary crystallization and the second one corresponds to the secondary crystallization which occurs in the interlamellar regions (once spherulites are in contact one with the other). An influence of the temperature is noted for both methods of isothermal crystallization which leads to a variation on the Avrami's exponent as shown in Table 4.

At annealing temperatures of 120 °C and 125 °C, the crystallization rates are high since crystallization half-time ($t_{1/2}$) are short: 2.25 and 0.8 min, respectively. The determined n values are close to 2 that indicates a heterogeneous two dimensional growth of crystals. This heterogeneous nucleation is probably due to the low value of the initial crystallinity ratio of our material which can be considered as preferential locations for nucleation [59]. However, at lower annealing temperature ($T = 115$ °C), n is close to 4 and $t_{1/2}$ is close to 5 min. The crystallization rate is then very low even if there are preferential sites for nucleation. Regarding the n value, the nucleation is homogeneous with a three-dimensional crystals growth.

Consequently, the crystals nucleation and growth modes are linked to the crystallization rate and thus to annealing temperature. The higher the temperature, the higher the

Table 3 Characteristic temperatures determined by DSC and Raman spectroscopy

Heating rate (°C/min)	DSC			Raman Spectroscopy		
	T_g (°C)	T_{cc} (°C)	T_f (°C)	T_g (°C)	T_{cc} (°C)	T_f (°C)
2.5	74	122	248	75	123	249
5	76	125	247	76	126	248
10	77	132	245	77	133	246
15	78	136	245	79	137	245
20	80	140	244	80	140	244

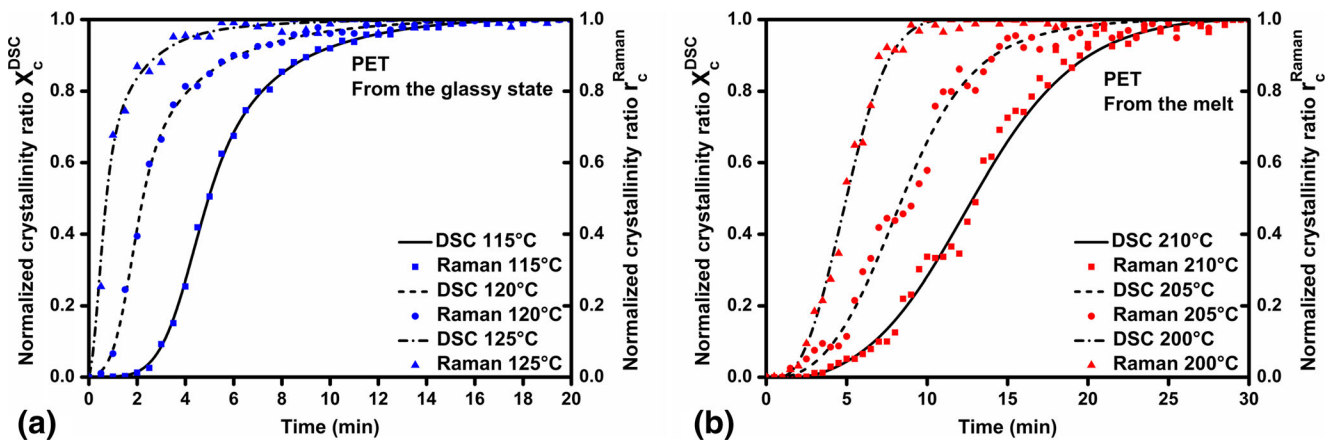


Fig. 8 Evolutions of the crystallinity ratio as a function of the time by Raman spectroscopy and DSC: **a** annealing from the glassy state and **b** cooling from the melt

molecular mobility and then higher is the crystallization rate. But, a fast crystallization leads to imperfect crystals which are localized essentially in the initial nucleation sites because at high temperatures the nucleation is disadvantaged. At the opposite, the molecular mobility is difficult at lower temperatures which favor the nucleation process to the detriment of the crystallization rate. So, the influence of the crystallites initially present in the material is very low.

Considering the isothermal crystallinity from the melt, two different types of crystallization are observed: primary and secondary crystallization. For the primary crystallization, the average value of n is close to 4 which mean that, from the melt where the material is completely amorphous, we are in the case of homogeneous nucleation with a three-dimensional growth. The second type is characterized by an average value of n close to 3 describing a

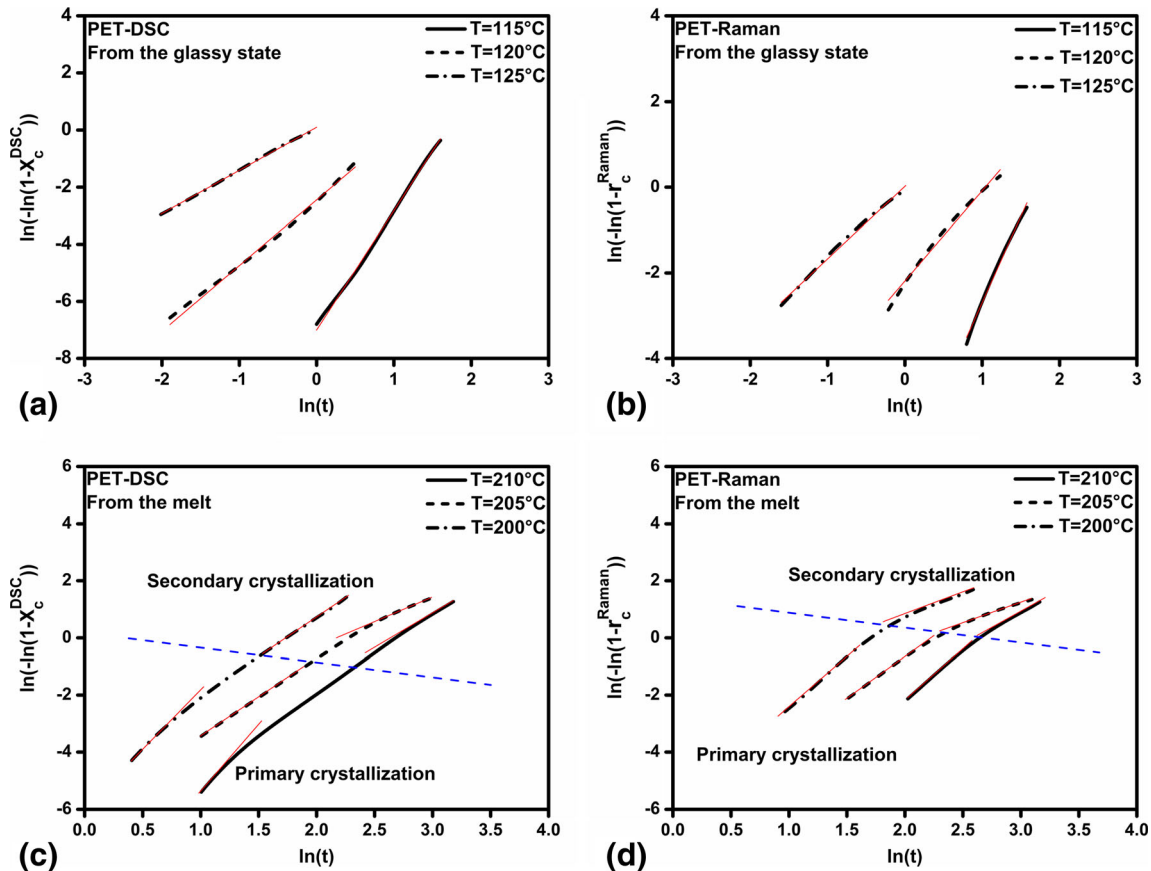


Fig. 9 Comparison between the Avrami's plots for the PET determined by DSC and Raman spectroscopy: **a, b** annealing from the glassy state and **c, d** cooling from the melt

Table 4 Avrami's exponent n and $t_{1/2}$ obtained by data analysis from Raman spectroscopy and DSC for the two methods of isothermal crystallization

		T(°C)	$t_{1/2}$ (min)	Avrami exponent n	
				Primary crystallization	Secondary crystallization
From the glassy state	Raman spectroscopy	115	4.98	4	–
		120	2.25	2.1	–
		125	0.8	1.9	–
	DSC	115	4.95	4.2	–
		120	2.23	2.3	–
		125	0.73	1.7	–
From the melt	Raman spectroscopy	200	4.93	3.6	1.6
		205	8.35	3	1.3
		210	12.78	3.8	2.3
	DSC	200	4.98	3.9	2.5
		205	8.41	3.1	1.7
		210	12.85	4.2	2.7

heterogeneous nucleation occurring in the interlamellar zones of the spherulites formed during the first step of crystallization (primary crystallization). In addition, it is noticed that the shorter the $t_{1/2}$, the faster the crystallization rate. The crystallization half-time increases with temperature. At high crystallization temperature, the supercooling

degree is lower which leads to difficulties in the formation of nuclei.

Thus homogeneous nucleation with a three dimensional growth can be obtained either from the amorphous form (melted material) or from an initial low crystallized material annealed with a low crystallization rate.

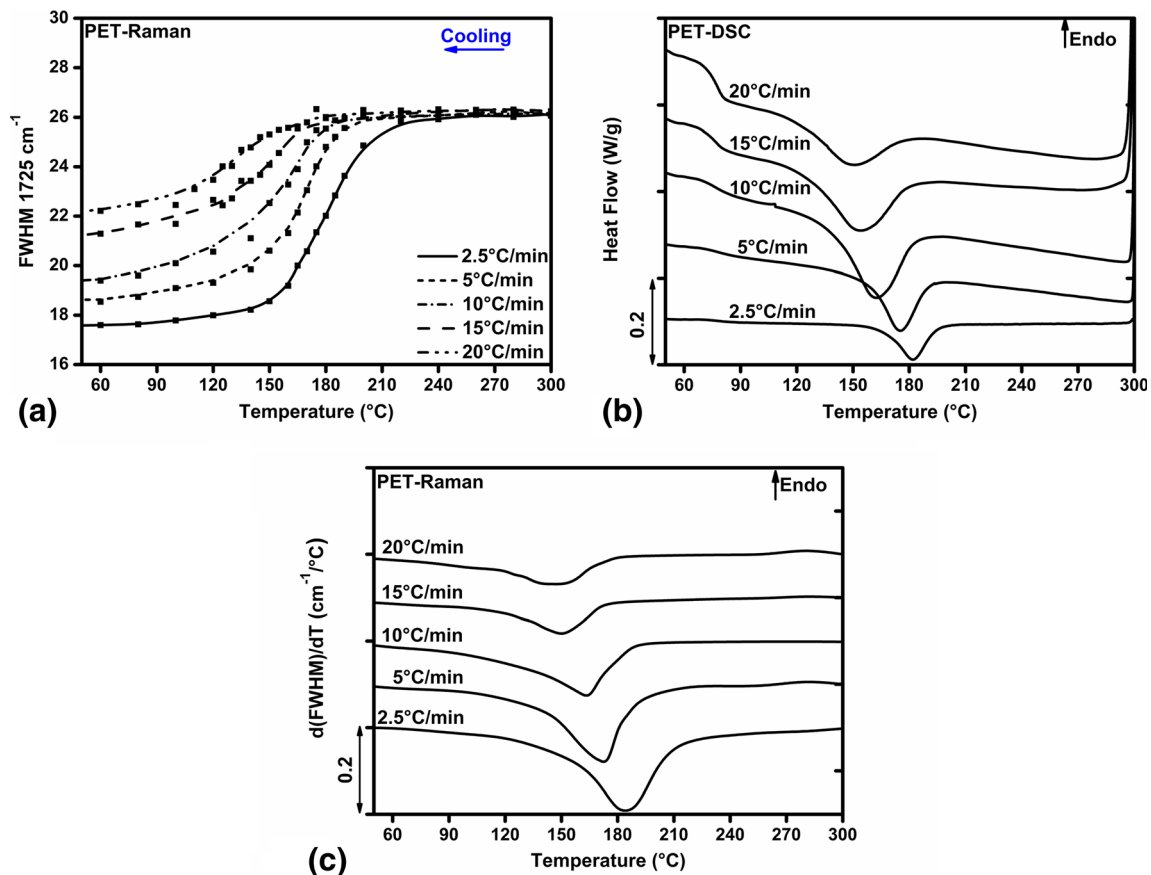


Fig. 10 Evolutions of **a** FWHM of the carbonyls vibrational band, **b** Heat flow and **c** $\frac{d(\text{FWHM})}{dT}$ as a function of temperature for different cooling rates

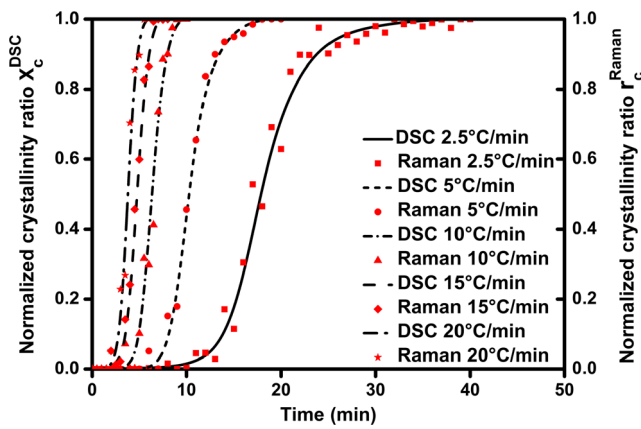


Fig. 11 Evolutions of the crystallinity ratio as a function of time by Raman spectroscopy and DSC for the non-isothermal crystallization

The values of n and the crystallization half-time $t_{1/2}$ obtained by Raman spectroscopy are in complete agreement with those obtained by DSC.

Non-isothermal crystallization

To describe the non-isothermal crystallization of PET, Ozawa theory, extension of the Avrami's, is used to validate the proposed Raman crystallinity criterion and test if the Raman results are in agreement with those obtained by the DSC method.

The evolution of the FWHM and $\frac{d(FWHM)}{dT}$ of the carbonyl groups vibrational band are plotted as a function of temperature at each cooling rate (Fig. 10).

As it is noticed in Fig. 5(d) and Fig. 6, the FWHM which describes the environmental disorder in the material, is too sensitive to the characteristic temperatures. Figure 10(a) shows the evolution of the bandwidth of 1725 cm^{-1} vibrational bands. At the beginning of the cooling procedure, the FWHM value is 26 cm^{-1} corresponding to the same value obtained after heating to melting. With decreasing temperature, FWHM decreases more or less rapidly depending on the cooling rate which describes an organization of the

macromolecular structure of the material. At 2.5 °C/min (low cooling rate), the FWHM reaches the value of 17.8 cm^{-1} against 22.3 cm^{-1} at 20 °C/min (high cooling rate). These values correspond respectively to a high and low crystallinity ratio which confirms the dependence of this vibrational band on the macromolecular arrangement and cooling or heating rates. Indeed, Fig. 10(c) shows a complete agreement between the $\frac{d(FWHM)}{dT}$ obtained by Raman spectroscopy with the Heat Flow evolutions from DSC data (Fig. 10(b)). The crystallization temperatures follow the same evolution whether if they are determined by one or the other technique. The temperatures correspond to the inflection point of the FWHM curves.

Figure 11 shows the evolution of the crystallinity determined by DSC and by Raman spectroscopy using the Raman ratio r_c^{Raman} . As it has been observed earlier, the results obtained from those two technics are in complete agreement.

In order to determine the nucleation modes for the crystallization of the PET from the melt, the Ozawa's equation is linearized by considering a double logarithm. $\ln(-\ln(1-X_c))$ is then plotted as a function of $\ln C$ where C corresponds to the different crystallization rates (2.5, 5, 10, 15 and 20 °C/min). It is usually predicted that Ozawa plots for the dynamic crystallization describe straight lines at each temperature [28, 35] but in Fig. 12, two kinetic regimes are identified. As it is observed applying Avrami's theory, these two regimes correspond to a primary crystallization process at low crystallinity fraction and a secondary crystallization process at high crystallinity fraction. It is also noticed that the fractional crystallinity corresponding to the change of slope increases with increasing temperature describing a linear function of temperature (red dashed lines in Fig. 12).

The temperatures used to conduct the Ozawa analysis of non-isothermal crystallization are 210 °C , 190 °C , 170 °C and 150 °C . Non-isothermal study reveals a complete agreement between the Ozawa exponent values either if they are determined by Raman spectroscopy or by DSC (Table 5).

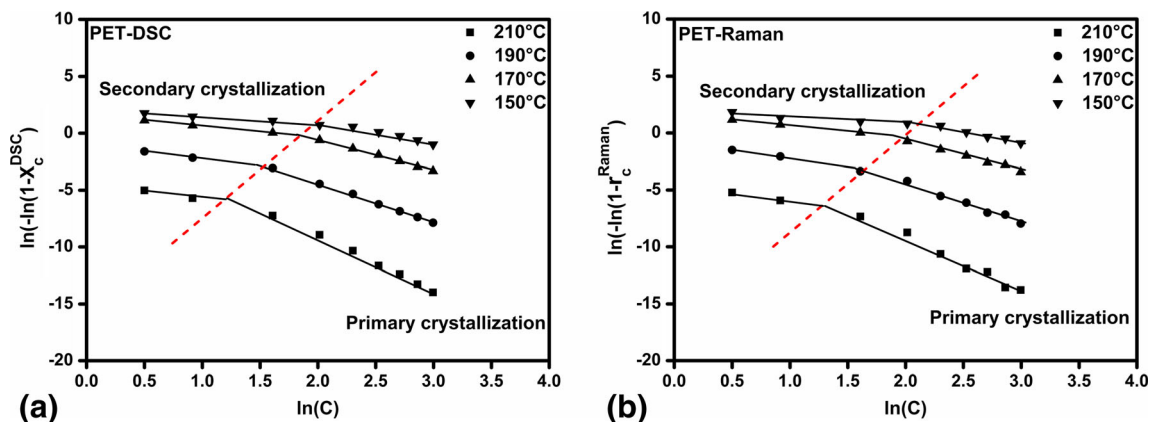


Fig. 12 Ozawa plots for non-isothermal crystallization of PET determined by a DSC and b Raman spectroscopy

Table 5 Ozawa exponent m obtained by data analysis from Raman spectroscopy and DSC

T(°C)	Ozawa exponent m			
	Raman spectroscopy		DSC	
	Primary crystallization	Secondary crystallization	Primary crystallization	Secondary crystallization
210	4.8	1.7	4.9	1.66
190	3.3	1.35	3.5	1.32
170	2.5	1.01	2.8	0.96
150	2.4	0.63	2.5	0.62

An influence of the temperature on the Ozawa exponent is noted. Indeed, m increases with increasing temperature. The same trend had already been observed for isothermal crystallization from the melt (Table 4). As it is described in Table 5 for the primary crystallization, at higher temperature (well above crystallization temperature), growth rate is low which favors homogeneous nucleation with a three dimensional growth (m value is close to 4). At 170 °C and 150 °C, the average m value is rather close to 3 corresponding to a heterogeneous three dimensional growth. This behavior is due to the nucleation sites that are already in progress because at these both temperatures, the crystallization has already started whatever the value of the cooling rate (Fig. 10(b)). For the secondary crystallization, m increases with the temperature. At 150 °C, 170 °C and 190 °C, the average value of m is close to 1 corresponding to a heterogeneous one dimensional crystallization occurring in the interlamellar zones of the spherulites at the end of the crystallization process. But at 210 °C, m is rather close to 2 which correspond to a heterogeneous two dimensional growth occurring also in the interlamellar zones of the spherulites in order to complete the crystallization procedure. This m value (close to 2) corresponds to the same result at 210 °C obtained by Avrami's theory applied during an isothermal crystallization from the melt.

Conclusion

In this paper, in situ Raman acquisitions during controlled thermal treatments ensured by the DSC apparatus have allowed us a real-time monitoring of the microstructural evolutions that occur in the PET material.

Following the 1725 cm^{-1} vibrational band allowed to highlight the importance of the carbonyls in the description of the regularity and the disorder occurring in the polymer during thermal treatments. In addition, the characteristic temperatures of the material are easily determined. Thanks to the 1096 cm^{-1} vibrational band evolutions, quantifying the degree of

crystallinity of PET with a good precision by using the r_c^{Raman} Raman ratio, is now possible by performing a Raman scan.

Furthermore, Raman measurements allowed us to determine Avrami and Ozawa exponents by performing isothermal and non-isothermal measurements. Ozawa and Avrami expressions play an important role in the study of the crystallization kinetic especially when techniques such as Raman spectroscopy are used. According to some studies, n and m do not correlate with the crystallization temperatures [60–62], but our results prove that the opposite occurs.

Raman spectroscopy has been able to detect all the changes that happen when thermal treatments are applied to a polymer material in addition to the vibrational informations. The examination of kinetics and all the changes that occur at the functional group level has been possible using this new approach.

As a perspective to our study, crystallinity, nucleation modes and even characteristic temperatures of a polymer material can be determined during an extrusion process as an example using Raman spectroscopy as a real time monitoring probe.

Acknowledgments We are grateful to Kaiser Optical System for lending us the Raman probe adapted to the DSC oven to ensure Raman measurement during DSC scan.

References

1. Lee B, Shin TJ, Lee SW, Yoon J, Kim J, Youn HS, Ree M (2003) Time-resolved X-ray scattering and calorimetric studies on the crystallization behaviors of poly(ethylene terephthalate) (PET) and its copolymers containing isophthalate units. *Polymer* 44(8):2509–2518. doi:10.1016/s0032-3861(03)00130-7
2. Kong Y, Hay J (2002) The measurement of the crystallinity of polymers by DSC. *Polymer* 43(14):3873–3878
3. Asano A, Tanaka C, Murata Y (2007) NMR determination of crystallinity for poly (ϵ -l-lysine). *Polymer* 48(13):3809–3816
4. Hagemann H, Snyder R, Peacock A, Mandelkern L (1989) Quantitative infrared methods for the measurement of crystallinity and its temperature dependence: polyethylene. *Macromolecules* 22(9):3600–3606
5. Melveger A (1972) Laser-raman study of crystallinity changes in poly (ethylene terephthalate). *J Polym Sci Part A-2: Polym Phys* 10(2):317–322
6. Koenig J (1971) Raman scattering of synthetic polymers—a review. *Appl Spectrosc Rev* 4(2):233–305
7. Hollas JM (2004) *Modern spectroscopy*. Wiley
8. Gerrard D, Maddam W (1986) Polymer characterization by Raman spectroscopy. *Appl Spectrosc Rev* 22(2–3):251–334
9. Edwards H, Johnson A, Lewis I (1993) Applications of Raman spectroscopy to the study of polymers and polymerization processes. *J Raman Spectrosc* 24(8):475–483
10. Chalmers J, Edwards H, Lees J, Long D, Mackenzie M, Willis H (1991) Raman spectra of polymorphs of isotactic polypropylene. *J Raman Spectrosc* 22(11):613–618
11. Lippert T, Zimmermann F, Wokaun A (1993) Surface analysis of excimer-laser-treated polyethylene-terephthalate by surface-

- enhanced Raman scattering and x-ray photoelectron spectroscopy. *Appl Spectrosc* 47(11):1931–1942
12. Cole KC, Aji A, Pellerin E (2002) New insights into the development of ordered structure in poly (ethylene terephthalate), II Results from transmission infrared spectroscopy of thin films. In: *Macromolecular Symposia*, vol 1. Wiley Online Library, pp 1–18
 13. Jarvis D, Hutchinson I, Bower D, Ward I (1980) Characterization of biaxial orientation in poly (ethylene terephthalate) by means of refractive index measurements and Raman and infra-red spectroscopies. *Polymer* 21(1):41–54
 14. Yang S, Michielsen S (2003) Orientation distribution functions obtained via polarized Raman spectroscopy of poly (ethylene terephthalate) fibers. *Macromolecules* 36(17):6484–6492
 15. Yang S, Michielsen S (2004) Analysis of the 1030-cm⁻¹ band of poly (ethylene terephthalate) fibers using polarized raman microscopy. *J Polym Sci B Polym Phys* 42(1):47–52
 16. Kawakami D, Hsiao BS, Burger C, Ran S, Avila-Orta C, Sics I, Kikutani T, Jacob KI, Chu B (2005) Deformation-induced phase transition and superstructure formation in Poly(ethylene terephthalate). *Macromolecules* 38(1):91–103. doi:10.1021/ma049333x
 17. Lin W, Cossar M, Dang V, Teh J (2007) The application of Raman spectroscopy to three-phase characterization of polyethylene crystallinity. *Polym Test* 26(6):814–821. doi:10.1016/j.polymertesting.2007.05.004
 18. Strobl G, Hagedorn W (1978) Raman spectroscopic method for determining the crystallinity of polyethylene. *J Polym Sci Polym Phys Ed* 16(7):1181–1193
 19. Ponçot M, Martin J, Hiver JM, Verchère D, Dahoun A (2012) Study of the dimensional instabilities of laminated polypropylene films during heating treatments. *J Appl Polym Sci* 125(5):3385–3395. doi:10.1002/app.36450
 20. Martin J, Ponçot M, Hiver JM, Bourson P, Dahoun A (2013) Real-time Raman spectroscopy measurements to study the uniaxial tension of isotactic polypropylene: a global overview of microstructural deformation mechanisms. *J Raman Spectrosc* 44(5):776–784. doi:10.1002/jrs.4244
 21. Chaudemanche S, Ponçot M, André S, Dahoun A, Bourson P (2014) Evolution of the Raman backscattered intensity used to analyze the micromechanisms of deformation of various polypropylene blends in situ during a uniaxial tensile test. *J Raman Spectrosc* 45(5):369–376. doi:10.1002/jrs.4463
 22. Song L, Ma W, Ren Y, Zhou W, Xie S, Tan P, Sun L (2008) Temperature dependence of Raman spectra in single-walled carbon nanotube rings. *Appl Phys Lett* 92(12):121905. doi:10.1063/1.2891870
 23. Colomban P (2002) *Imagerie Raman de matériaux et dispositifs hétérogènes*. Techniques de l'Ingénieur
 24. McGraw GE (1970) Study of molecular orientation in poly (ethylene terephthalate) fibers by fluorescence polarization. *J Polym Sci Part A-2: Polym Phys* 8(8):1323–1336
 25. McGraw G (1970) Paper presented at American chemical society meeting. *Polym Prepr* 11:1122
 26. Bulkin BJ, Lewin M, DeBlase FJ (1985) Conformational change, chain orientation, and crystallinity in poly (ethylene terephthalate) yarns: Raman spectroscopic study. *Macromolecules* 18(12):2587–2594
 27. Wei L, Jiang J, Shan M, Chen W, Deng Y, Xue G, Zhou D (2014) Integration of ultrafast scanning calorimetry with micro-Raman spectroscopy for investigation of metastable materials. *Rev Sci Instrum* 85(7):074901. doi:10.1063/1.4889882
 28. Papageorgiou GZ, Achilias DS, Bikiaris DN, Karayannidis GP (2006) Isothermal and non-isothermal crystallization kinetics of branched and partially crosslinked PET. *J Therm Anal Calorim* 84(1):85–89. doi:10.1007/s10973-005-7366-4
 29. Chen Z, Hay JN, Jenkins MJ (2013) The kinetics of crystallization of poly(ethylene terephthalate) measured by FTIR spectroscopy. *Eur Polym J* 49(6):1722–1730. doi:10.1016/j.eurpolymj.2013.03.020
 30. Bulkin BJ, Lewin M, McKelvy ML (1985) Crystallization kinetics of poly(ethylene terephthalate) studied by rapid scanning Raman spectroscopy. *Spectrochim Acta A: Mol Spectrosc* 41(1–2):251–261. doi:10.1016/0584-8539(85)80103-3
 31. Balkanski M, Haro E, Espinosa GP, Phillips JC (1984) Raman scattering study of glass crystallization kinetics. *Solid State Commun* 51(8):639–642. doi:10.1016/0038-1098(84)91078-0
 32. Keller A, Lester G, Morgan L (1954) Crystallization phenomena in polymers. I. Preliminary investigation of the crystallization characteristics of polyethylene terephthalate. *Philos Trans R Soc Lond A Math Phys Eng Sci* 247(921):1–12
 33. Mayhan K, James W, Bosch W (1965) Poly (ethylene terephthalate). I Study of crystallization kinetics. *J Appl Polym Sci* 9(11):3605–3616
 34. Bertoldo M, Labardi M, Rotella C, Capaccioli S (2010) Enhanced crystallization kinetics in poly(ethylene terephthalate) thin films evidenced by infrared spectroscopy. *Polymer* 51(16):3660–3668. doi:10.1016/j.polymer.2010.05.040
 35. Ghasemi H, Carreau PJ, Kamal MR (2012) Isothermal and non-isothermal crystallization behavior of PET nanocomposites. *Polym Eng Sci* 52(2):372–384. doi:10.1002/pen.22092
 36. Lee B, Lee JW, Lee SW, Yoon J, Ree M (2004) Synthesis and non-isothermal crystallization behavior of poly(ethylene phthalate-co-terephthalate)s. *Polym Eng Sci* 44(9):1682–1691. doi:10.1002/pen.20168
 37. Porter RS (1980) *Macromolecular physics, volume 3—crystal melting*, Bernhard Wunderlich. Academic Press, New York, p. 363 Price: \$42.50. Wiley Online Library
 38. Mehta A, Gaur U, Wunderlich B (1978) Equilibrium melting parameters of poly (ethylene terephthalate). *J Polym Sci Polym Phys Ed* 16(2):289–296
 39. Long DA (2005) In: Chalmers JM, Griffiths PR (eds) *Handbook of vibrational spectroscopy*, vol 1–5. John Wiley & Sons, Chichester, 2002, p 3862
 40. Khafagy RM (2006) In situ FT-Raman spectroscopic study of the conformational changes occurring in isotactic polypropylene during its melting and crystallization processes. *J Polym Sci B Polym Phys* 44(15):2173–2182
 41. Avrami M (1939) Kinetics of phase change. I general theory. *J Chem Phys* 7(12):1103–1112
 42. Avrami M (1940) Kinetics of phase change. II transformation-time relations for random distribution of nuclei. *J Chem Phys* 8(2):212–224
 43. Avrami M (1941) Kinetics of phase change. III. Granulation, phase change, and microstructure. *J Chem Phys* 9(2):177–184
 44. Ozawa T (1971) Kinetics of non-isothermal crystallization. *Polymer* 12(3):150–158
 45. Štokr J, Schneider B, Doskočilová D, Lövy J, Sedláček P (1982) Conformational structure of poly(ethylene terephthalate). Infra-red, Raman and n.m.r. spectra. *Polymer* 23(5):714–721. doi:10.1016/0032-3861(82)90057-x
 46. Ellis G, Roman F, Marco C, Gomez M, Fatou J (1995) FT Raman study of orientation and crystallization processes in poly (ethylene terephthalate). *Spectrochim Acta A Mol Biomol Spectrosc* 51(12):2139–2145
 47. Daubeny RdP, Bunn C (1954) The crystal structure of polyethylene terephthalate. In: *Proceedings of the Royal Society of London A: Mathematical, Physical and Engineering Sciences*, vol 1167. The Royal Society, pp 531–542
 48. Manley T, Williams D (1969) Structure of terephthalate polymers I—infra-red spectra and molecular structure of poly (ethylene terephthalate). *Polymer* 10:339–384
 49. Ward I, Wilding M (1977) Infra-red and Raman spectra of poly (m-methylene terephthalate) polymers. *Polymer* 18(4):327–335

50. Stuart B (1996) Polymer crystallinity studied using Raman spectroscopy. *Vib Spectrosc* 10(2):79–87
51. Paquin R, Limage M-H, Colombari P (2007) Micro-Raman study of PET single fibres under high hydrostatic pressure: phase/conformation transition and amorphization. *J Raman Spectrosc* 38(9):1097–1105. doi:10.1002/jrs.1716
52. Liang C, Krimm S (1959) Infrared spectra of high polymers: part IX. Polyethylene terephthalate. *J Mol Spectrosc* 3(1):554–574
53. Colombari P, Corset J (1999) Foreword to the special issue on Raman(micro) spectrometry and materials science. *J Raman Spectrosc* 30(10):863–866
54. Everall N, Tayler P, Chalmers J, MacKerron D, Ferwerda R, Van der Maas J (1994) Study of density and orientation in poly (ethylene terephthalate) using Fourier transform Raman spectroscopy and multivariate data analysis. *Polymer* 35(15):3184–3192
55. Young R (1997) Analysis of composites using Raman and fluorescence microscopy—a review. *J Microsc* 185(2):199–205
56. Huang Y, Young RJ (1994) Analysis of the fragmentation test for carbon-fibre/epoxy model composites by means of Raman spectroscopy. *Compos Sci Technol* 52(4):505–517
57. Gouadec G, Colombari P (2007) Raman spectroscopy of nanomaterials: how spectra relate to disorder, particle size and mechanical properties. *Prog Cryst Growth Charact Mater* 53(1):1–56. doi:10.1016/j.pcrysgrow.2007.01.001
58. Manley T, Williams D (1971) The infra-red spectrum and molecular structure of poly (cyclohexane 1, 4-dimethylene terephthalate). *Polymer* 12(1):2–26
59. Sajkiewicz P (2002) Transient and athermal effects in the crystallization of polymers. I. Isothermal crystallization. *J Polym Sci B Polym Phys* 40(17):1835–1849
60. Mitsuishi Y, Ikeda M (1966) Studies on crystallization of poly (ethylene terephthalate) by differential thermal analysis. Special consideration of the two exothermic peaks in the thermogram of crystallization. *J Polym Sci Part A-2: Polym Phys* 4(2):283–288
61. Collier JR, Baer E (1966) Crystallization from the glassy state. *J Appl Polym Sci* 10(10):1409–1419
62. Sun T, Pereira J, Porter RS (1984) Crystallization kinetics for poly (ethylene terephthalate) oriented by solid-state coextrusion. *J Polym Sci Polym Phys Ed* 22(7):1163–1171